Chinese Journal of Natural Medicines

Tianxiangdan (TXD) alleviates myocardial ischemia reperfusion-induced ferroptosis through the activation of estrogen receptor alpha (ER α)

Yuanjia Yue, Yu Li, Xing Rong, Zhao Ji, Huimin Wang, Liang Chen, Lin Jiang

Citation: Yuanjia Yue, Yu Li, Xing Rong, Zhao Ji, Huimin Wang, Liang Chen, Lin Jiang, Tianxiangdan (TXD) alleviates myocardial ischemia reperfusion-induced ferroptosis through the activation of estrogen receptor alpha (ER α), Chinese Journal of Natural Medicines, 2025, 23(1), 102-110. doi: 10.1016/S1875-5364(25)60811-9.

View online: https://doi.org/10.1016/S1875-5364(25)60811-9

Chinese Journal of Natural Medicines 23 (2025) 102-110

Contents lists available at ScienceDirect

Chinese Journal of Natural Medicines

journal homepage: www.cjnmcpu.com/

Original article

Tianxiangdan (TXD) alleviates myocardial ischemia reperfusion-induced ferroptosis through the activation of estrogen receptor alpha (ERα)

Yuanjia Yue[a,b,c], Yu Li[d], Xing Rong[a], Zhao Ji[a], Huimin Wang[a], Liang Chen[a,b], Lin Jiang[a,b,*]

[a] *Department of Pharmacy, The Fourth College of Clinical Medicine, Xinjiang Medical University, Urumqi 830000, China*
[b] *Department of Pharmacy, Xinjiang Uygur Autonomous Region Hospital of Traditional Chinese Medicine, Urumqi 830000, China*
[c] *State Key Laboratory of Pathogenesis, Prevention and Treatment of High Incidence Diseases in Central Asia, Xinjiang Medical University , Urumqi 830000, China*
[d] *Department of Neurosurgery ICU, Xinjiang Uygur Autonomous Region People's Hospital, Urumqi, 830000, China*

ARTICLE INFO

Article history:
Received 29 March 2024
Revised 14 May 2024
Accepted 1 July 2024
Available online 20 January 2025

Keywords:
Tianxiangdan
Estrogen receptor alpha
Ferroptosis
Myocardial ischemia-reperfusion injury
Network pharmacology

ABSTRACT

Tianxiangdan (TXD), a traditional Chinese herbal remedy, demonstrates efficacy in mitigating myocardial ischemia-reperfusion (I/R)-induced damage. This study employed network pharmacology to evaluate the therapeutic targets and mechanisms of TXD in treating I/R. High-performance liquid chromatography-mass spectrometry (HPLC-MS) identified 86 compounds in TXD. Network pharmacological analysis predicted potential target genes and their modes of action. Cardiac function, ischaemic ST changes, lactate dehydrogenase (LDH), malondialdehyde (MDA), superoxide dismutase (SOD) activity, myocardial fiber, and infarct size were assessed using *in vivo* and *in vitro* I/R injury models. Estrogen receptor alpha (ERα) protein expression and estradiol (E2) levels were measured to confirm TXD's impact on estrogen levels and ERα expression. To examine if TXD reduces I/R injury through ERα, an AZD group (300 nmol·L^{-1} AZD9496 and 15% TXD serum) was compared to a TXD group (15% TXD serum). The study hypothesized that TXD upregulates the ERα-mediated iron metamorphosis pathway. I/R injury-induced ferroptosis was identified using a Fer-1 group (1.0 μmol·L^{-1} Fer-1 and 15% TXD serum) to elucidate the potential association between ferroptosis and ERα proteins. A DCFH-DA probe detected reactive oxygen species (ROS) and Fe^{2+}, while Western blotting assessed target protein expression. Both *in vitro* and *in vivo* experiments demonstrated that TXD attenuated I/R injury by reducing elevated ST-segment levels, improving cardiac injury biomarkers (LDH, MDA, and SOD), alleviating pathological features, and preventing I/R-induced loss of cell viability *in vitro*. The effects and mechanisms of TXD on I/R injury-associated ferroptosis were investigated using I/R-induced H9c2 cells. The TXD group showed significantly decreased ROS and Fe^{2+} levels, while the AZ group (treated with AZD9496) exhibited increased levels. The TXD group demonstrated enhanced expression of ERα and glutathione peroxidase 4 (GPX4), with reduced levels of P53 protein and ferritin-heavy polypeptide 1 (FTH1). The AZ group exhibited contrasting effects on these expression levels. The literature indicated a novel connection between ERα and ferroptosis. TXD activates the ERα signaling pathway, promoting protection against I/R-induced myocardial cell ferroptosis. This study provides evidence supporting TXD use for myocardial ischemia treatment, particularly in older female patients who may benefit from its therapeutic outcomes.

1. Introduction

Heart failure represents a significant public health challenge, with its prevalence increasing in recent years. This trend may be attributed to an aging population and improved survival rates among patients with coronary artery disease (CAD) [1]. Acute myocardial infarction (AMI), a severe cardiac condition, primarily results from thrombus formation obstructing coronary arteries [2]. The standard treatment for AMI involves rapid restoration of blood flow to the coronary arteries. However, clinical observations frequently indicate that myocardial damage exacerbates during the reperfusion phase, leading to myocardial ischemia-reperfusion (I/R) injury [3]. Despite the high morbidity and poor prognosis associated with I/R, effective prevention and treatment strategies remain elusive, necessitating urgent research attention. This study investigates the pathogenesis of I/R and explores therapeutic approaches using Chinese patent medicines.

Research indicates that women face a higher risk of heart failure following myocardial infarction. Furthermore, the prevalence of hypertension in women increases with age [4]. Menopausal hypertensive patients often experience greater blood pressure fluctuations. Additionally, compared to patients with convention-

* Corresponding author.
E-mail address: 597900175@qq.com

https://doi.org/10.1016/S1875-5364(25)60811-9

al cardiovascular disease, older women may exhibit elevated pulse pressure and disorders in glucose and lipid metabolism. Consequently, achieving optimal therapeutic outcomes solely through antihypertensive treatment presents challenges [5]. Estradiol (E2) supplementation can be beneficial, as it promotes vasodilation, protects vascular endothelium, reduces blood pressure levels, and mitigates disease severity [6]. However, estrogen therapy may elevate the risk of breast and endometrial cancers. In contrast, hormone replacement therapy based on traditional Chinese medicine (TCM) can offer effective treatment with comparatively lower risk [7]. Moreover, due to potential health risks associated with hormone therapy, estrogen-activating agents are currently being utilized to treat myocardial ischemia in menopausal women.

Tianxiangdan (TXD) is a TCM formula that has been used for centuries, with historical accounts suggesting its formulation by Xunbang Zhang during the Ming Dynasty (14th century). In TCM, TXD is believed to tonify the heart and *Qi* (vital energy) while exhibiting calming and anti-inflammatory properties. In modern pharmacological research, TXD has gained interest for drug development and was approved for clinical trials as a novel Chinese medicine in 2015 (approval number: 2015L03185) [8]. TXD comprises water extracts of Rhodiolae Crenulatae Radix et Rhizoma (Hongjingtian), Dalbergiae Odoriferae Lignum (Jiangxiang), Small Leaf Ziziphora (Xintahua), and Salviae Miltiorrhizae Radix et Rhizoma (Danshen) in equal proportions (1∶1∶1∶1). Research has demonstrated that TXD exerts its effects against atherosclerosis *via* nuclear factor kappa B (NF-*κ*B) and p38 mitogen-activated protein kinases (p38/MAPK) signaling pathways, and improves coronary microvascular dysfunction (CMD) in rats by suppressing inflammation in the micro-vessels through nuclear factor erythroid 2-related factor 2 (Nrf2) activation [8, 9]. The pathogenesis of CAD is closely linked to atherosclerosis, CMD, and ischemia/reperfusion (I/R) injury. Furthermore, atherosclerosis can induce CMD, thereby substantially increasing the risk of myocardial I/R injury [10].

In this study, network pharmacology was employed to analyze the molecular interactions and target relationships between the active compounds of TXD and I/R. It integrates preliminary findings on the association of estrogen receptor alpha (ERα), ferroptosis, and TXD with current scientific insights to provide evidence for I/R therapy. Ferroptosis, an iron-dependent, non-apoptotic form of cell death, is primarily characterized by reactive oxygen species (ROS) accumulation. It plays a critical role in the pathophysiology of I/R injury, where it regulates key pathways involving ROS production, glutathione peroxidase 4 (GPX4), and autophagy-dependent ferroptosis pathways [11]. The aim of this research is to present evidence for treating I/R patients, particularly elderly women, with TXD, which could potentially improve therapeutic outcomes. This research aims to present evidence for treating I/R patients, particularly elderly women, with TXD, potentially improving therapeutic outcomes. The study highlights innovative approaches in TCM for myocardial ischemia treatment. It suggests that hormone replacement therapy derived from TCM could offer a safer and more effective solution for menopausal women, with reduced associated risks.

2. Materials and methods

2.1. Animals and ethical approval

A total of 80 SPF-grade SD rats (70 females and 10 males) were obtained from the Animal Experimental Center of Xinjiang Medical University (SCXK: 20220003). The study was approved by the Experimental Animal Ethics Committee of Xinjiang Medical University (Ethics approval number: IACUC-20210326-13) and conducted in full compliance with the ARRIVE (Animal Research: Reporting of *In Vivo* Experiments) guidelines.

2.2. Materials

TXD (20210816) was obtained from Xinjiang Autonomous Region Traditional Chinese Medicine Hospital (Xinjiang, China). Estrogen receptor inhibitor (S837201) was procured from Selleck (Houston, USA). Ferroptosis inhibitors (hy-100579) were acquired from MCE (New Jersey, USA). Bicinchoninic acid (BCA) kit (Prilley, CAS: p1511-1/2/3); cell counting kit-8 (CCK-8) kit (Abbkine, CAS: KTC011001); ROS kit (S0033s), lactate dehydrogenase (LDH) kit (C0016), superoxide dismutase (SOD) kit (S0101s) and malondialdehyde (MDA) kit (S0131s) were obtained from Biyuntian (Shanghai, China). Dulbecco's modified eagle medium (DMEM) (41420ES76) and pancreatic enzyme (40126ES60) were purchased from Yeasen (Shanghai, China). Fetal bovine serum (16000044) was acquired from GIBCO (Waltham, USA); P53 antibody (ab131442), ferritin-heavy polypeptide 1 (FTH1) antibody (ab266581), GPX4 antibody (ab144369) and goat anti-rabbit secondary antibody (ab150077) were obtained from Abcam (Shanghai, China). Salidroside (10338-51-9), tyrosol (501-94-0), and salvianolic acid B (121521-90-2) were procured from MCE (New Jersey, USA).

2.3. HPLC-MS analysis of TXD components

The components of TXD were analyzed using the Waters UPLC Xevo T Q-S micro (Waters Corporation, Milford, MA, USA). To prepare the TXD solution, 2.0 g of TXD powder was precisely weighed and combined with 20 mL of water. The mixture underwent water bath reflux extraction for 60 min, after which it was allowed to cool. Subsequently, the water quantity was adjusted to compensate for any weight loss, and the resulting solution was filtered.

The chromatographic analysis employed an ACQUITY UPLC HSS T3 column (2.1 mm × 100 mm, 1.8 μm). The mobile phase consisted of 0.1% formic acid aqueous solution (A) and acetonitrile (B). Gradient elution was performed at a column temperature of 40 °C and a flow rate of 0.25 mL·min^{-1}. The injection volume for gradient elution was 5 μL.

The ionization technique employed was electrospray ionization (ESI), utilized in both positive and negative ion detection modes. The mass spectrometer parameters were as follows: scanning range of mass-to-charge ratio (*m/z*) 50–1200; capillary voltage of 3.0 and 2.5 kV for positive and negative ion modes, respectively; cone hole voltage of 40 V; cone hole gas flow rate of 50 L·h^{-1}; desolvation gas flow rate of 900 L·h^{-1}; collision gas flow rate of 0.2 mL·min^{-1}; ionization source temperature of 150 °C; and desolvation gas temperature of 350 °C. The data acquisition method utilized was the Mississippi Educator Career (MSE) Continuum.

2.4. Prediction of targets and mechanisms of TXD-I/R *via* network pharmacology

GeneCards (http://www.genecards.org) was utilized to obtain target information for the chemical composition of TXD by high-performance liquid chromatography-mass spectrometry (HPLC-MS). Additionally, DisGeNET (https://www.disgenet.org/), Therapeutic Target Database (TTD, https://db.idrblab.net/ttd/), and the Online Mendelian Inheritance in Man (OMIM, http://omim.org) were employed with the disease keyword "myocardial ischemia" to acquire various disease targets related to myocardial ischemia. To identify potential co-acting targets for TXD-I/R, a Venny diagram was generated using Venny 2.0 *via* liuxiaoyuyuan.cn. The protein-protein interaction (PPI) network

was constructed using STRING (https://cn.string-db.org/) with TXD-I/R target inputs, setting the criteria as "Homo sapiens" and "highest confidence (> 0.9) ". Cytoscape3.9 (http://cytoscape.org/) was employed to visualize the network and generate TXD-chemical composition-target-myocardial ischemia maps. Gene Ontology (GO)-biofunction and Kyoto Encyclopedia of Genomes (KEGG) signaling pathways were screened in Metascape (http://metascape.org/) using TXD-I/R targets. In the DockThor platform (https://dockthor.lncc.br/), ERα underwent molecular docking with salidroside, which possessed the greatest amount of TXD moiety. The optimal conformation with the lowest docking binding energy was selected for analyzing the binding mode. The results were visualized using Pymol 2.3.0 software.

2.5. Establishment of ovariectomy (OVX) model

Rats were weighed and anesthetized *via* intraperitoneal injection of pentobarbital sodium (40 mg·kg^{-1}). The animals were positioned laterally on the operating table, and their muscle layer was carefully separated using blunt forceps to expose the ovary. The ovarian structure was observed to closely resemble a chrysanthemum in appearance. Using blunt forceps, the ovary was gently grasped, and a non-absorbable suture soaked in normal saline was introduced below it to create a secure ligation. The ovaries were then excised using ophthalmic scissors. Finally, an appropriate amount of penicillin powder was applied to the surgical site, which was subsequently closed with an absorbable suture, as previously described [12].

2.6. Establishment of myocardial I/R model

The female SD rats (n = 70) were initially anesthetized through intraperitoneal injection of pentobarbital sodium (40 mg·kg^{-1}). Their four limbs were then immobilized for electrocardiogram analysis *via* a standard lead II electrocardiograph. Following skin preparation of the left sternal rib, the pectoralis major muscle was meticulously dissected layer by layer using homeostatic forceps to expose the left atrial region of the heart. Subsequently, the left anterior descending atrium was ligated with a suture. The rats were then subjected to 30 min of ischemia followed by reperfusion [13]. In the Con (control) and OVX groups, the coronary artery remained unligated after threading, with other procedures mirroring those described above. Finally, heart tissues and serum were collected for subsequent experiments.

H9c2 cells were cultured in glucose-deficient DMEM and incubated in a 37 °C Tri-Gas incubator (1% O_2, 5% CO_2, and 94% N_2) for 6 h. Subsequently, the incubator conditions were adjusted to 95% air and 5% CO_2 for an additional 2 h [14].

2.7. Experimental design

Female SD rats (n = 70, age = 9 weeks old, weight = 210 ± 40 g) were maintained in the Experimental Animal Centre of Xinjiang Medical University under controlled conditions: room temperature (22 ± 2) °C, relative humidity of 50% ± 5%, and a 12 h alternating light and dark cycle. The rats were randomly assigned to 7 groups of 10 rats each, as indicated in the table (Fig. 1A). Additionally, H9c2 cells were cultured in DMEM supplemented with 5% fetal bovine serum and 100 unit·mL^{-1} penicillin in a humidified incubator at 37 °C with 95% air and 5% CO_2. These cells were subsequently divided randomly into seven distinct groups as outlined in the table (Fig. 1B).

2.8. Treatment with drug-containing serum

The TXD dosage was calculated based on the body surface area of humans and animals as well as the standard daily dosage for adults (TXD capsules, thrice daily, 4 capsules per administration). TXD capsules (0.378 g·kg^{-1}·d^{-1}) were administered for 4 consecutive days. Subsequently, male SD rats (n = 10) were anesthetized *via* intraperitoneal injection of pentobarbital sodium (40 mg·kg^{-1}). After 1 h, blood was collected from their abdominal aorta and left to stand at room temperature for 20 min. The supernatant was then centrifuged at 4 °C for 10 min at 1500 r·min^{-1}. Finally, the complement was inactivated in a water bath for 30 min, filtered through a 0.22 μm filter, aliquoted, and stored at −80 °C for future use.

2.9. Cardiac function data detection and collection

Female SD rats were fasted without water for 12 h prior to surgery. Anesthesia was induced by an intraperitoneal injection of sodium pentobarbital (40 mg·kg^{-1}), and the rats were positioned on the operating table. Then the neck and chest areas were disinfected using standard surgical protocols. A tracheotomy was then performed, followed by intubation, and the rats were connected to a ventilator (frequency = 65 beats/min, tidal volume = 18 mL, inspiratory-expiratory ratio = 2∶1). Finally, needles for electrode placement were inserted subcutaneously into the limbs, and the electrodes were connected to the BL-420S Biofunction Experiment System.

2.10. 2,3,5-Chlorophenyltetrazolium (TTC) staining of rat heart

The heart tissues, previously stained with Evans blue, were excised and subsequently sectioned into 2−3 mm circular slices from the base to the apex. These sections were then incubated at 37 °C in 1% TTC dye for 15 min, followed by fixation in 4% paraformaldehyde. Post-staining, the non-infarcted myocardial tissue in the at-risk area appeared red, while the infarcted zone was distinguishable by its white coloration.

2.11. Hematoxylin-eosin (HE) staining of rat's myocardium

Upon completion of the ischemic period, the cardiac tissues underwent fixation in 4% paraformaldehyde, followed by dehydration in ethanol. The tissues were then washed, embedded in paraffin, and subsequently in neutral gum. Hematoxylin staining was applied for 5 min, followed by eosin staining for 1 min. Finally, the samples were subjected to dehydration, neutral gum treatment, and transparency procedures before image acquisition.

2.12. Determination of LDH in rat blood

Following anesthesia, 2 mL of carotid blood was extracted from the rats and left to stand at room temperature for 2 h. Subsequently, the supernatant underwent centrifugation at 1 × 10^4 r·min^{-1} for 10 min at 4 °C. The LDH content was then measured according to the kit's protocol.

2.13. Measurement of MDA and SOD content in rat myocardial tissues

Frozen rat myocardial tissues underwent homogenization and subsequent centrifugation at 1 × 10^4 r·min^{-1} for 10 min. The resulting supernatant was collected for the determination of MDA and SOD levels, following the protocols specified in the respective assay kits.

2.14. Cell viability assessment *via* CCK-8 method

Following the grouping and treatment of H9c2 cells with various drugs at 37 °C in CO_2, a 5% CCK-8 solution was applied to

A

	Pre-adaptation	OVX	Administration	Hypoxia-ischemia	Reperfusion
Con					
OVX		+			
I/R		+		+	+
E2		+	0.8 mg·kg^{-1}·d^{-1} E2	+	+
TXD-H		+	0.8 mg·kg^{-1}·d^{-1} TXD	+	+
TXD-M		+	0.4 mg·kg^{-1}·d^{-1} TXD	+	+
TXD-L		+	0.2 mg·kg^{-1}·d^{-1} TXD	+	+
	7 d		60 d	30 min	30 min
	Subsequent treatment				

B

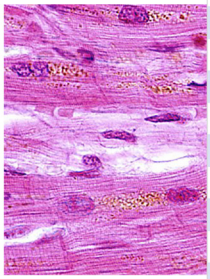

	Administration	Hypoxia	Reperfusion
Con			
I/R		+	+
AZ	300 nmol·L^{-1} AZD9496 + 15% TXD medicated serum	+	+
E2	10^{-8} mol·L^{-1} E2	+	+
TXD-H	15% TXD medicated serum	+	+
TXD-L	5% TXD medicated serum	+	+
Fer-1	1.0 μmol·L^{-1} Fer-1 + 15% TXD medicated serum	+	+
	24 h	6 h	2 h
	Subsequent treatment		

Fig. 1 The schematic representation of experimental grouping and corresponding treatment on (A) rat and (B) H9c2 cells.

the cells for 30 min, adhering to the detection kit instructions. Subsequently, the optical density values of cells in each group were measured using an enzyme-linked immunosorbent assay at 450 nm.

2.15. Determination of E2 in rat blood and H9c2 cells

Following anesthesia, 2 mL of carotid blood was collected from the rats and left to stand at room temperature for 2 h. The supernatant was subsequently centrifuged at 1 × 10^4 r·min^{-1} for 10 min at 4 °C, and the E2 content was measured according to the kit's protocol. After treatment of each cell group, the culture medium was removed, and the cells were washed three times with DMEM. The E2 content was then determined following the kit's instructions. At the conclusion of the incubation period, the absorbance values of each cell group were measured using an enzyme marker.

2.16. Determination of Fe^{2+} in H9c2 cells

Following the treatment of each cell group, the culture medium was removed and the cells were rinsed three times with DMEM. The Fe^{2+} content was measured according to the kit's protocol. At the conclusion of the incubation period, the absorbance values for each cell group were observed using enzyme markers.

2.17. Detection of ROS by DCFH-DA probe in H9c2 cells

Upon reaching 80%–90% confluency, the H9c2 cells were grouped and modeled. Subsequently, 1 mL of probe containing DCFH-DA (1 × 10^{-4} mol·L^{-1}) was introduced and incubated for 30 min at room temperature. The treated cells were then examined and imaged using a Leica TCS SP8 X laser confocal microscope (E_x: 488 nm, E_m: 525 nm).

2.18. Western blotting analysis

EProtein extraction was performed on H9c2 cells and myocardial lysates obtained from the anterior wall of the left ventricle. The protein concentration was subsequently determined using the BCA protein quantification kit. Equal quantities of protein were then separated on Bolt™ 4 to 12% BisTris protein gels for 80 min and transferred to PVDF membranes for 50 min. The membranes were incubated with primary antibodies in a refrigerated shaker at 4 °C for 12 h, washed three times with PBS for 10 min each, and then treated with secondary antibodies. Finally, an electrochemical luminescence (ECL) reagent was applied to visualize the protein bands. The resulting band intensities were analyzed using ImageJ software to determine relative protein levels.

2.19. Statistical processing

The data are presented as mean ± SD and analyzed using GraphPad Prism 9.0 software. The differences among multiple groups were analyzed by one-way analysis of variance. A *P*-value < 0.05 was considered statistically significant.

3. Results

3.1. Detection of the main components of TXD by HPLC

HPLC-MS is a sophisticated analytical technique that combines the separation capabilities of liquid chromatography with the structural analysis prowess of mass spectrometry. Its notable advantages, including high specificity and sensitivity, make it particularly suitable for analyzing complex systems [15]. In this study, HPLC-MS was utilized to analyze the chemical components in the TXD capsule, identifying 86 promising components for future clinical trials and subsequent drug development. A superior peak shape indicates higher column efficiency and improved separation. The column's separation capacity reflects its ability to differentiate targets (peaks); thus, enhanced separation facilitates easier baseline separation between two peaks [16]. TXD demonstrated good and consistent peak shape and separation, with detection completed within a retention time of approximately 50 min (no additional peaks were observed after 50 min). The primary com-

ponents of TXD were identified as: 1. daidzein; 2. miltirone; 3. isomucronustyrene; 4. liquiritigenin; 5. rosmarinic acid; 6. salidroside; 7. salvianic acid A; 8. rutin; 9. kaempferide; 10. linarin; 11. cryptotanshinone; 12. lithospermic acid; 13. formononetin (Fig. S1, Table S1).

3.2. Candidate targets of TXD and myocardial I/R injury-induced ferroptosis

Molecular docking plays a critical role in virtual screening by accurately predicting favorable binding configurations between ligands and protein binding sites based on energy considerations. This approach enables the ranking and prioritization of compounds based on predicted binding affinities. In this study, 1599 myocardial ischemia targets were identified through screening the OMIM and DisGeNET databases, while 257 targets were found by searching the HPLC/MS-based chemical composition of TXD on TTD (Fig. 2A). The intersection of drug and myocardial ischemia targets yielded 84 common targets, which were then imported into the STRING database to generate a PPI network (Fig. 2B). Additionally, GO (Fig. 2C) and KEGG (Fig. 2D) enrichment analyses were conducted on the selected targets. Upon observing a potential correlation between ferroptosis and ERα, the study investigated TXD's potential to enhance E2 and ERα expression in ovariectomized rats. The initial hypothesis posited that ERα might regulate the ferroptosis pathway. Finally, molecular docking visualization was performed between ERα and salidroside, the latter being the most abundant component of TXD (Fig. 2E).

3.3. TXD therapy can protect the heart against I/R-induced damage in rats

Persistent elevation of ischemic ST segment alterations, as evidenced by electrocardiographic analysis, indicates the presence of myocardial ischemia [17]. During an ischemic event, these ST changes increase progressively for 30 min before gradually stabilizing following reperfusion. The study demonstrates that both TXD and E2 significantly mitigated the magnitude of ischemic ST changes (Fig. 3A).

TTC staining functions as a crucial marker for myocardial ischemia [18]. In this study, extensive myocardial infarction was observed in the I/R group, which was significantly mitigated by TXD and E2 administration (Fig. 3B).

The myocardial sections in the I/R group demonstrated significant pathological changes compared to the control group, as anticipated. These changes included disorganized myocardial fiber arrangement, partial myocardial fiber rupture and dissolution, myocardial cell edema, cell gap expansion, and substantial inflammatory cell infiltration. However, TXD and E2 treatments notably mitigated these symptoms (Fig. 3C). Previous research has established that serum LDH levels serve as a molecular indicator of myocardial injury [19], while SOD and MDA function as markers of oxidative stress. Consequently, measuring the serum concentrations of SOD, LDH, and MDA allows for the assessment of their content. The results revealed that, in comparison to the control group, the I/R group exhibited significantly elevated concentrations of LDH and MDA, whereas SOD concentrations were markedly reduced ($P < 0.05$). Following TXD and E2 pretreatment, however, LDH and MDA concentrations decreased significantly, while SOD concentrations increased substantially ($P < 0.05$) (Fig. 3D). Furthermore, the serum concentrations of SOD, LDH, and MDA in the TXD pretreatment group demonstrated correlation. These findings indicate that TXD effectively prevents I/R-induced injury.

3.4. Effects of TXD on E2 levels and ERα protein expression in rats and H9c2 cells

AZD9496 pre-treatment was observed to significantly reduce ERα protein expression levels in H9c2 cells. Notably, compared to the Con group, the I/R group exhibited significantly decreased ERα protein expression; however, TXD treatment re-

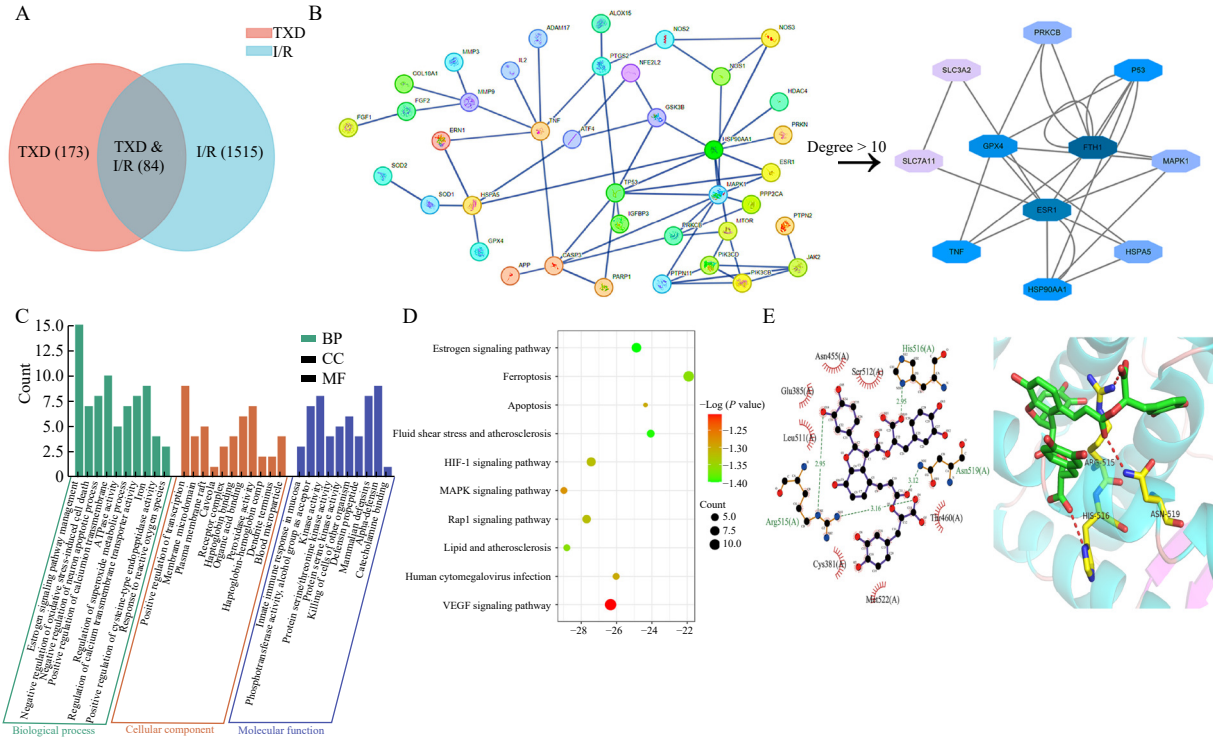

Fig. 2 Candidate targets of TXD and myocardial I/R injury-induced ferroptosis. (A) Venn diagram, (B) PPI network, (C) GO functional analysis and (D) KEGG signaling pathway of TXD-I/R. (E) Molecular docking of salidroside and ERα.

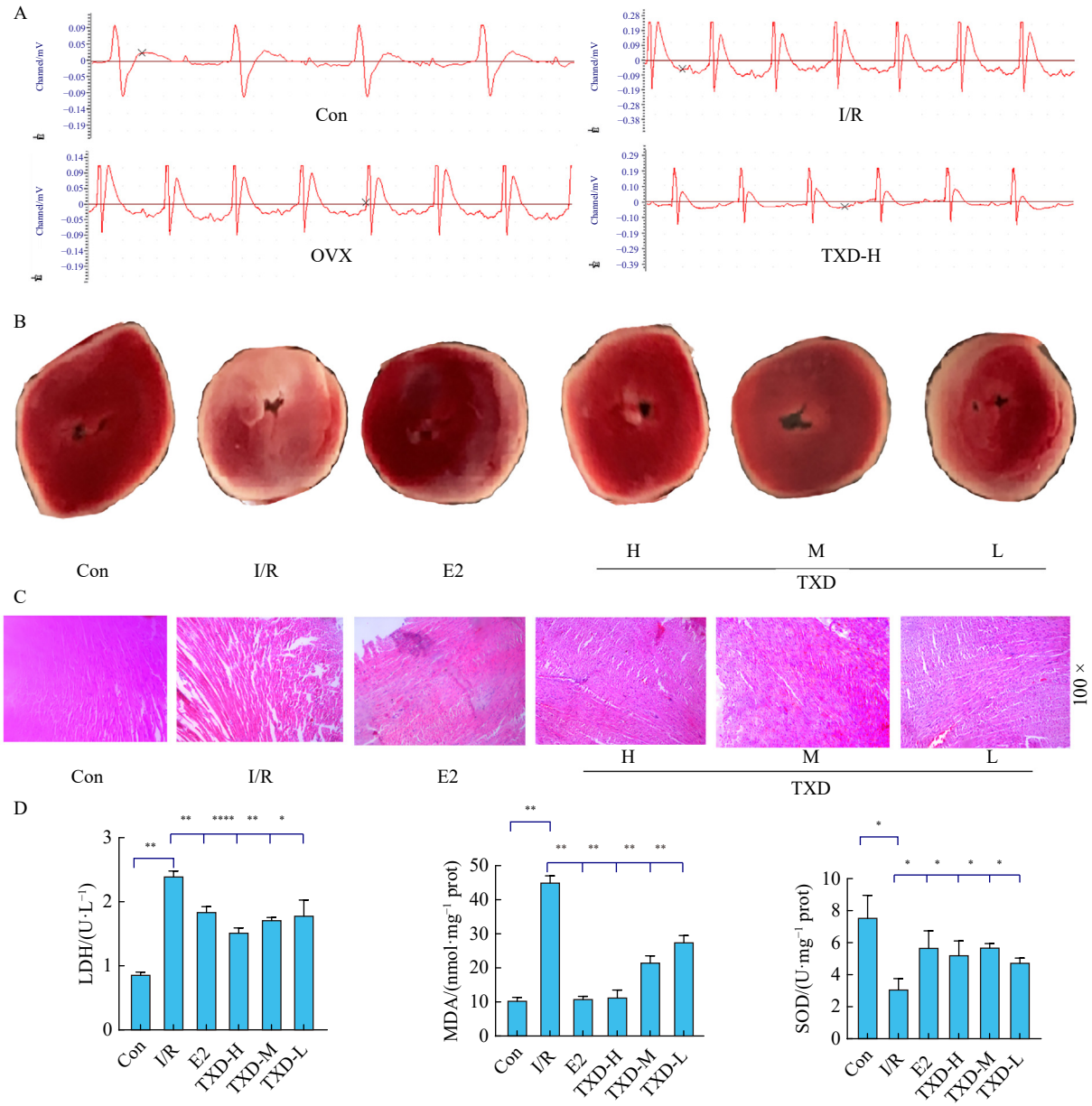

Fig. 3 Effects of TXD on heart protection. (A) Detection of ischemic ST changes by ECG. (B) Myocardial infarction size determined by TTC staining. (C) HE staining revealed distinct pathological changes in the heart myocardium. (D) Molecular indicators of myocardial injury and markers of oxidative stress. Data are expressed as mean ± SD (n = 3). $^{*}P < 0.05$, $^{**}P < 0.01$, $^{****}P < 0.0001$.

versed this effect in both H9c2 cells ($P < 0.05$) (Fig. 4A) and in rats ($P < 0.05$) (Fig. 4B). The TXD group demonstrated significantly higher E2 levels in both H9c2 and rat cells compared to the I/R group ($P < 0.05$) (Figs. 4C and 4D).

3.5. TXD alleviates I/R-induced damage by reducing ferroptosis through ERα upregulation in H9c2 cells

In the TXD group, the level of ROS was significantly lower compared to the I/R group. Additionally, ROS levels increased significantly after AZ pretreatment. TXD effectively prevented I/R-induced myocardial injury by inhibiting ROS levels (Fig. 5A). Western blotting analysis detected the expression of various proteins associated with ferroptosis and ERα after AZ and Fer-1 pretreatment. The expression levels of P53, GPX4, and FTH1 were significantly higher in the TXD group compared to the I/R group ($P < 0.05$). Furthermore, the expression of P53, GPX4, and FTH1 increased significantly after AZ pretreatment ($P < 0.05$), indicating that ERα could be used to treat I/R-induced ferroptosis (Fig. 5B). Moreover, a significant increase in Fe^{2+} content was observed in H9c2 cells in the I/R group compared to the control group ($P < 0.05$), suggesting a correlation between I/R and ferroptosis. Notably, compared to the TXD-H group, the AZ group significantly promoted ferroptosis progression ($P < 0.05$) (Fig. 5C). The CCK-8 assay, examining H9c2 cell activity, revealed that AZ group cell proliferation activity was markedly inhibited, which TXD and Fer-1 treatment reversed ($P < 0.05$). These results suggest that ferroptosis is the primary factor behind I/R injury. Additionally, the AZ group indicated that ERα plays a significant role in protecting I/R cells from ferroptosis (Fig. 5D). In conclusion, these findings demonstrate that TXD pretreatment significantly upregulates ERα expression and reduces ferroptosis in H9c2 cells injured by I/R.

4. Discussion

TCM offers several advantages, including multi-level and multi-target approaches with fewer adverse reactions. It has

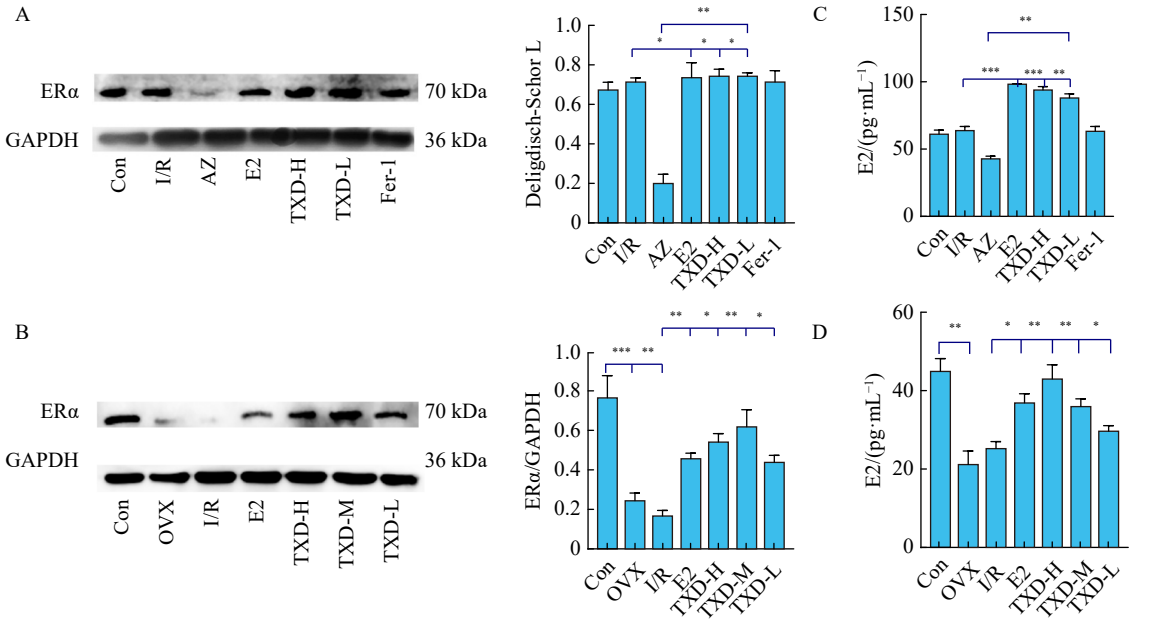

Fig. 4 Effects of TXD on E2 levels and ERα protein expression. Impact of TXD on ERα expression in (A) H9c2 cells and (B) rats. Effect of TXD on E2 levels in (C) H9c2 cells and (D) rats. Data are presented as mean ± SD (n = 3). $^{*}P < 0.05$, $^{**}P < 0.01$, $^{***}P < 0.001$.

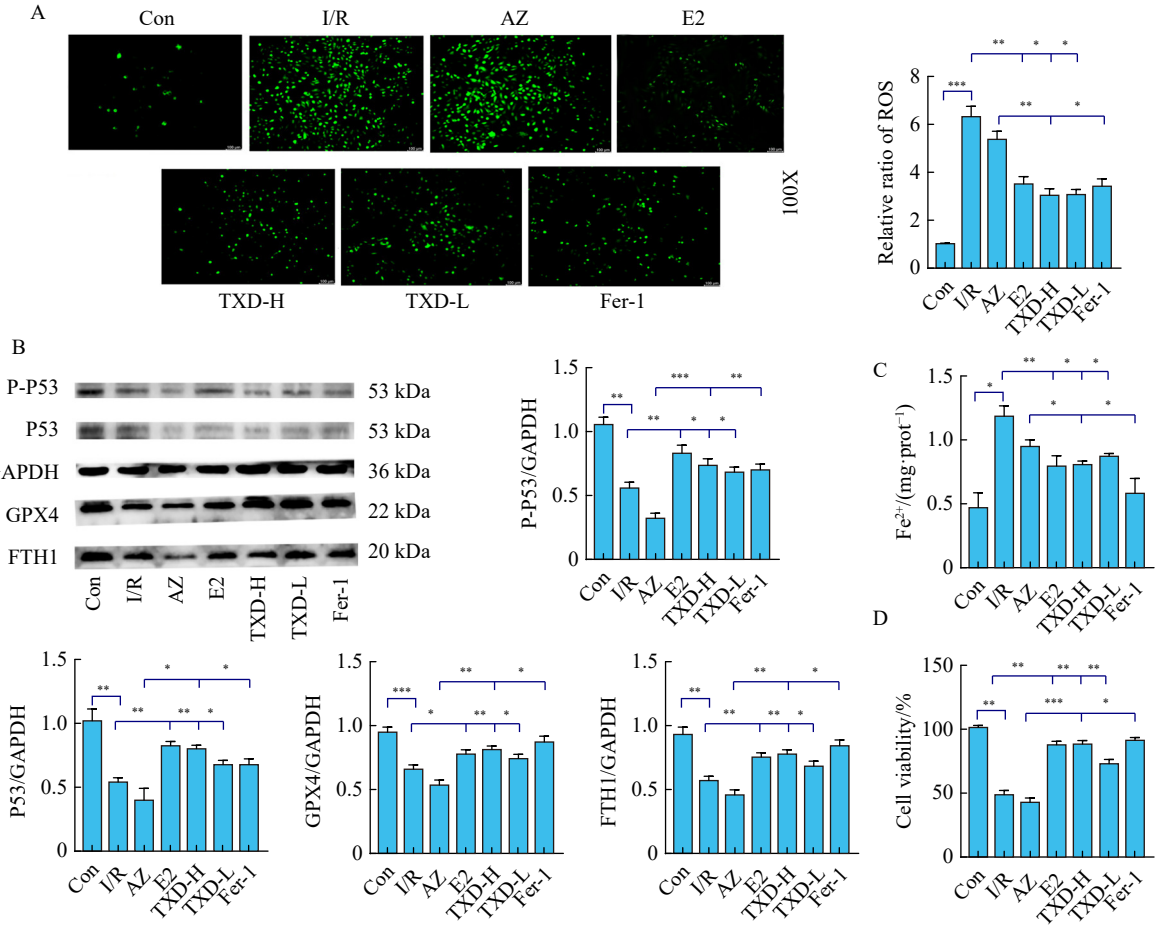

Fig. 5 TXD alleviates I/R-induced damage by reducing ferroptosis. (A) DCFH-DA was utilized to analyze ROS levels. (B) Western Blotting was conducted to examine the association between ERα and Ferroptosis-related proteins. (C) Measurement of Fe^{2+} content in H9c2 cells. (D) The viability of H9c2 cells was assessed using CCK-8 assay. The data are presented as mean ± SD (n = 3). $^{*}P < 0.05$, $^{**}P < 0.01$, $^{***}P < 0.001$.

demonstrated therapeutic effects against myocardial ischemia-reperfusion (I/R) injury through complex mechanisms. Due to its intricate composition, diverse mechanisms of action, and versatility, TCM represents a highly potent system. Consequently, promoting TCM for treating myocardial ischemia-reperfusion injury can significantly contribute to new drug research and development. TXD comprises Rhodiolae Crenulatae Radix et Rhizoma (Hongjingtian), Dalbergiae Odoriferae Lignum (Jiangxiang), Small

Leaf Ziziphora (Xintahua), and Salviae Miltiorrhizae Radix et Rhizoma (Danshen). Its primary active compound, salidroside, has been reported to have myocardial protective effects [20]. Furthermore, extracts from Danshen and Hongjingtian, as well as Jiangxiang, have been commonly utilized in treating myocardial ischemia and other cardiovascular diseases [21]. Additionally, the Uygur medicine Xintahua has shown efficacy in treating hypertension, edema, heart disease, insomnia, tracheitis, and hemorrhoids [22].

Salidroside treatment has been shown to significantly increase estrogen levels and decrease urinary calcium excretion, thus mitigating the deterioration of trabecular bone in OVX mice and diabetic mice [23]. Research indicates that salidroside can alleviate estrogen deficiency-induced osteoporosis and diabetes by elevating estrogen levels [24]. This investigation demonstrated that E2 concentration and ERα protein levels in the OVX group were markedly lower compared to the Con group; however, TXD treatment substantially increased these levels. Consequently, TXD appears to influence the estrogen signaling pathway, enabling estrogen to perform its normal functions.

Antioxidants and associated enzymes play a crucial role in preventing cardiovascular diseases. SOD is instrumental in maintaining the body's oxidative and antioxidant equilibrium by neutralizing superoxide anions, thereby shielding cells from oxidative stress-induced damage [25]. The human body generates oxygen-free radicals through both enzymatic and non-enzymatic processes, leading to lipid peroxidation and the production of metabolites such as MDA. Consequently, SOD activity levels serve as an indirect indicator of the body's capacity to neutralize oxygen-free radicals [26]. Additionally, MDA concentration levels indirectly reflect the extent of cellular damage caused by oxygen-free radical attacks. Oxidation can significantly impair blood vessel endothelial cells, facilitating the entry of low-density lipoprotein (LDL) [27]. Furthermore, oxidation can enhance blood clotting factor activity, promoting thrombus formation. Notably, treatment with TXD and E2 in I/R rats increased SOD activity while markedly reducing LDH and MDA levels. Therefore, TXD may mitigate various pathological damage to cardiac tissues by modulating oxidative stress injury through estrogen-like effects.

In most gynecologic cancers, estrogen disrupts intracellular iron homeostasis and promotes free iron export into the systemic circulation. ROS serve as crucial regulators of systemic iron balance. A study on a female mouse model demonstrated that estrogen significantly reduces ROS expression [28]. Furthermore, an *in vivo* investigation revealed that serum ROS levels decreased by more than 40% in women receiving E2 treatment [29]. Activation of estrogen-related receptor gamma can also enhance the effect of ferroptosis in sorafenib-resistant cells [30]. The present study identified a correlation between E2 and ferroptosis, observing that reduced E2 levels in a de-ovulated rat model resulted in more severe myocardial injury, which was substantially mitigated following E2 administration. This research is the first to demonstrate that ERα can effectively regulate ferroptosis and that AZD9496-induced ERα inhibition promotes ferroptosis-associated protein expression and hypoxic injury in H9c2 cells.

Excessive intracellular iron accumulation can induce lipid peroxidation. FTH1 plays a crucial role in reducing intracellular free iron and mitigating cell damage by maintaining Fe^{2+} homeostasis and preventing its overload. Notably, FTH1 knockout in cardiac tissues has been shown to disrupt iron regulation and increase cardiac oxidative stress, thereby heightening the risk of cardiac injury due to iron overload [31]. The susceptibility of cells to ferroptosis is primarily regulated by ROS and GPX4 [32]. GPX4 inhibits ferroptosis by converting toxic lipid ROS into non-toxic lipid alcohols in the presence of glutathione (GSH) [33]. In this study, a potential association between TXD and ferroptosis was observed. Furthermore, p53 expression and ROS levels were elevated in the I/R group, inducing ferroptosis in cardiomyocytes, which aligns with previous research findings. Moreover, TXD significantly reduced Fe^{2+} and ROS levels, as well as the expression of GPX4 and FTH1, while AZ demonstrated opposite effects. These findings suggest that TXD exerts a protective effect against I/R-induced cardiomyocyte ferroptosis by activating the ERα signaling pathway.

In conclusion, this study demonstrates that TXD exhibits a significant protective effect against hypoxia-induced cardiac damage and exerts cardioprotection by activating ERα to mitigate oxidative stress in myocardial tissues. Consequently, targeting ERα or key proteins involved in ferroptosis emerges as a crucial strategy for the prevention and treatment of myocardial ischemia. TXD presents potential as a therapeutic agent for managing myocardial ischemia in elderly women.

Funding

This research was supported by the National Natural Science Foundation of China (No. 8196140154), the Natural Science Foundation of Xinjiang Uygur Autonomous Region (Nos. 2023D01C139 and 2023D01C63), and the State Key Laboratory of Pathogenesis, Prevention and Treatment of High Incidence Diseases in Central Asia Fund (No. SKL-HIDCA-2020-8).

Declaration of competing interest

These authors have no conflict of interest to declare.

Supporting information

Supporting information for this study can be obtained by contacting the corresponding authors *via* E-mail.

References

1 Pagliaro BR, Cannata F, Stefanini GG, et al. Myocardial ischemia and coronary disease in heart failure. *Heart Fail Rev*. 2020;25(1):53–65. https://doi.org/10.1007/s10741-019-09831-z.
2 Hu L, Sun Y, Zhang H, et al. Catalpol ameliorates myocardial I/R injury through PI3k/Akt/P53 signaling-mediated anti-autophagy and anti-apoptosis. *Pharmacogn Mag*. 2023;19(4):946–953. https://doi.org/10.1177/09731296231189557.
3 Gibbons RJ. Myocardial ischemia in the management of chronic coronary artery disease: past and present. *Circ Cardiovasc Imaging*. 2021;14(1):e011615. https://doi.org/10.1161/CIRCIMAGING.120.011615.
4 Pratush A, Ye X, Yang Q, et al. Biotransformation strategies for steroid estrogen and androgen pollution. *Appl Microbiol Biotechnol*. 2020;104(6):2385–2409. https://doi.org/10.1007/s00253-020-10374-9.
5 Wilkinson HN, Hardman MJ. The role of estrogen in cutaneous ageing and repair. *Maturitas*. 2017;103:60–64. https://doi.org/10.1016/j.maturitas.2017.06.026.
6 Chen K, Wang S, Sun QW, et al. Klotho deficiency causes heart aging *via* impairing the Nrf2-GR pathway. *Circ Res*. 2021;128(4):492–507. https://doi.org/10.1161/CIRCRESAHA.120.317348.
7 Deligdisch-Schor L. Hormone therapy effects on the uterus. *Adv Exp Med Biol*. 2020;1242:145–177.
8 Jiang L, Yue YJ, Tang M, et al. Mechanism investigation of Tianxiangdan against myocardial ischemia based on network pharmacology, molecular docking, and *in vitro* experimental. *Pharmacogn Mag*. 2024;20(3):784–793. https://doi.org/10.1177/09731296231220992.
9 Sun LF, An DQ, Niyazi GL, et al. Effects of Tianxiangdan Granule treatment on atherosclerosis *via* NF-κB and p38 MAPK signaling pathways. *Mol Med Rep*. 2018;17(1):1642–1650. https://doi.org/10.3892/mmr.2017.8067.
10 Wang WW, Liu XL, Ding Y, et al. Scutellarin protects myocardial ischemia-reperfusion injury ERK1/2-CREB regulated mitophagy. *Pharmacogn Mag*. 2023;19(4):1021–1036. https://doi.org/10.1177/09731296231199860.
11 Liang D, Minikes AM, Jiang X. Ferroptosis at the intersection of lipid metabolism and cellular signaling. *Mol Cell*. 2022;82(12):2215–2227. https://doi.org/10.1016/j.molcel.2022.03.022.
12 Sophocleous A, Idris AI. Ovariectomy/orchiectomy in rodents. *Methods Mol Biol*. 2019;1914:261–267. https://doi.org/10.1007/978-1-4939-8997-3_13.
13 Zhao W, Wu Y, Ye F, et al. Tetrandrine ameliorates myocardial ischemia reperfusion injury through miR-202-5p/TRPV2. *Biomed Res Int*. 2021;2021:8870674. https://doi.org/10.1155/2021/8870674.
14 Qiu Z, He Y, Ming H, et al. Lipopolysaccharide (LPS) aggravates high glucose- and hypoxia/reoxygenation-induced injury through activating ROS-dependent NLRP3 inflammasome-mediated pyroptosis in H9C2 cardiomyocytes. *J Diabetes Res*. 2019;2019:8151836. https://doi.org/10.

1155/2019/8151836.
15 Tang D, Wang C, Gan Q, et al. Chemical composition-based characterization of the anti-allergic effect of Guominkang Formula on IgE-mediated mast cells activation and passive cutaneous anaphylaxis. *Chin J Nat Med*. 2022;20(12): 925–936. https://doi.org/10.1016/S1875-5364(22)60225-5.
16 Xia H, Zhang JF, Wang LY, et al. Bioactive neolignans and lignans from the roots of *Paeonia lactiflora*. *Chin J Nat Med*. 2022;20(3):210–214. https://doi.org/10.1016/S1875-5364(22)60164-X.
17 Hayıroğlu M, Lakhani I, Tse G, et al. In-hospital prognostic value of electrocardiographic parameters other than ST-segment changes in acute myocardial infarction: literature review and future perspectives. *Heart Lung Circ*. 2020;29(11):1603–1612. https://doi.org/10.1016/j.hlc.2020.04.011.
18 Yan HF, Tuo QZ, Yin QZ, et al. The pathological role of ferroptosis in ischemia /reperfusion-related injury. *Zool Res*. 2020;41(3):220–230. https://doi.org/10.24272/j.issn.2095-8137.2020.042.
19 Liam CCK, Tiao JY, Yap YY, et al. Validating lactate dehydrogenase (LDH) as a component of the PLASMIC predictive tool (PLASMIC-LDH). *Blood Res*. 2023;58 (1):36–41. https://doi.org/10.5045/br.2023.2022133.
20 Gerbarg PL, Brown RP. Pause menopause with *Rhodiola rosea*, a natural selective estrogen receptor modulator. *Phytomedicine*. 2016;23(7):763–769. https://doi.org/10.1016/j.phymed.2015.11.013.
21 Li Z, Liu M, Chen M, et al. Clinical effect of Danshen Decoction in patients with heart failure: a systematic review and meta-analysis of randomized controlled trials. *PLoS One*. 2023;18(5):e0284877. https://doi.org/10.1371/journal.pone.0284877.
22 Whaley AO, Ivkin DY, Zhaparkulova KA, et al. Chemical composition and cardiotropic activity of *Ziziphora clinopodioides* subsp. bungeana (Juz.) Rech. f. *J Ethnopharmacol*. 2023;315:116660. https://doi.org/10.1016/j.jep.2023.116660.
23 Chen XF, Li XL, Yang M, et al. Osteoprotective effects of salidroside in ovariectomized mice and diabetic mice. *Eur J Pharmacol*. 2018;819:281–288. https://doi.org/10.1016/j.ejphar.2017.12.025.
24 Zheng H, Qi S, Chen C. Salidroside improves bone histomorphology and prevents bone loss in ovariectomized diabetic rats by upregulating the OPG/RANKL ratio. *Molecules*. 2018;23(9):2398. https://doi.org/10.3390/molecules23092398.
25 Wang C, Yuan W, Hu A, et al. Dexmedetomidine alleviated sepsis-induced myocardial ferroptosis and septic heart injury. *Mol Med Rep*. 2020;22(1): 175–184. https://doi.org/10.3892/mmr.2020.11114.
26 Liu Y, Shu J, Liu T, et al. Nicorandil protects against coronary microembolization-induced myocardial injury by suppressing cardiomyocyte pyroptosis *via* the AMPK/TXNIP/NLRP3 signaling pathway. *Eur J Pharmacol*. 2022;936:175365. https://doi.org/10.1016/j.ejphar.2022.175365.
27 Pálóczi J, Paál Á, Pigler J, et al. Organ-specific model of simulated ischemia/reperfusion and hyperglycemia based on engineered heart tissue. *Vascul Pharmacol*. 2023;152:107208. https://doi.org/10.1016/j.vph.2023.107208.
28 Yang L, Wang H, Yang X, et al. Auranofin mitigates systemic iron overload and induces ferroptosis *via* distinct mechanisms. *Signal Transduct Target Ther*. 2020;5(1):138. https://doi.org/10.1038/s41392-020-00253-0.
29 Yang WS, SriRamaratnam R, Welsch ME, et al. Regulation of ferroptotic cancer cell death by GPX4. *Cell*. 2014;156(1-2):317–331. https://doi.org/10.1016/j.cell.2013.12.010.
30 Kim HS, Seo JY, Park NG. Material and device stability in perovskite solar cells. *ChemSusChem*. 2016;9(18):2528–2540. https://doi.org/10.1002/cssc.201600915.
31 Liang D, Feng Y, Zandkarimi F, et al. Ferroptosis surveillance independent of GPX4 and differentially regulated by sex hormones. *Cell*. 2023;186(13): 2748–2764.e2722. https://doi.org/10.1016/j.cell.2023.05.003.
32 Bai Y, Wang W, Wang L, et al. Obacunone attenuates liver fibrosis with enhancing anti-oxidant effects of GPx-4 and inhibition of EMT. *Molecules*. 2021;26(2):318. https://doi.org/10.3390/molecules26020318.
33 Dang R, Wang M, Li X, et al. Edaravone ameliorates depressive and anxiety-like behaviors *via* Sirt1/Nrf2/HO-1/Gpx4 pathway. *J Neuroinflammation*. 2022;19(1):41. https://doi.org/10.1186/s12974-022-02400-6.